Check for updates

High-frequency linear rheology of hydrogels probed by ultrasound-driven microbubble dynamics

Akaki Jamburidze,[a] Marco De Corato,[a] Axel Huerre, [ID] [a] Angelo Pommella[b] and Valeria Garbin [ID] *[a]

Ultrasound-driven microbubble dynamics are central to biomedical applications, from diagnostic imaging to drug delivery and therapy. In therapeutic applications, the bubbles are typically embedded in tissue, and their dynamics are strongly affected by the viscoelastic properties of the soft solid medium. While the behaviour of bubbles in Newtonian fluids is well characterised, a fundamental understanding of the effect on ultrasound-driven bubble dynamics of a soft viscoelastic medium is still being developed. We characterised the resonant behaviour in ultrasound of isolated microbubbles embedded in agarose gels, commonly used as tissue-mimicking phantoms. Gels with different viscoelastic properties were obtained by tuning agarose concentration, and were characterised by standard rheological tests. Isolated bubbles (100–200 μm) were excited by ultrasound (10–50 kHz) at small pressure amplitudes (<1 kPa), to ensure that the deformation of the material and the bubble dynamics remained in the linear regime. The radial dynamics of the bubbles were recorded by high-speed video microscopy. Resonance curves were measured experimentally and fitted to a model combining the Rayleigh–Plesset equation governing bubble dynamics, with the Kelvin–Voigt model for the viscoelastic medium. The resonance frequency of the bubbles was found to increase with increasing shear modulus of the medium, with implications for optimisation of imaging and therapeutic ultrasound protocols. In addition, the viscoelastic properties inferred from ultrasound-driven bubble dynamics differ significantly from those measured at low frequency with the rheometer. Hence, rheological characterisation of biomaterials for medical ultrasound applications requires particular attention to the strain rate applied.

1 Introduction

Biomedical applications of ultrasound-driven microbubbles include diagnostic imaging[1] and drug delivery.[2] In these applications, micron-sized gas bubbles are injected intravenously and remain confined in the blood vessels. For therapeutic purposes, microbubbles can be delivered to tissues, for instance by acoustic droplet vaporisation,[3,4] or bubbles can be generated directly inside tissues, for instance in high-intensity focused ultrasound and lithotripsy.[5–7] The behaviour of bubbles embedded in tissues has been exploited for diagnostic purposes to measure the rheological properties of the tissue, such as in tissue palpation and elastography.[8] In these methods, ultrasound with frequency far above the resonance frequency of the bubbles is applied, to avoid bubble oscillations and only cause a displacement due to

acoustic radiation force.[9–11] The rheological properties extracted from these methods are therefore at a strain rate of 0 Hz. If the ultrasound frequency is close to the bubble resonance frequency, a bubble undergoes oscillatory behaviour, and imposes much larger strain rates on the surrounding medium, up to 10^6 Hz. The oscillatory deformation could therefore be utilised to measure rheological properties in a regime of deformation that is central to imaging and therapeutic ultrasound. However, while the oscillatory dynamics of bubbles in Newtonian fluids is well characterised,[12] our understanding of ultrasound-driven bubble dynamics in viscoelastic media is still limited.

Extensive theoretical work has been done on bubble dynamics in viscoelastic media. Most models are based on extensions of the Rayleigh–Plesset equation, taking into account viscosity, elasticity, and compressibility of the surrounding medium, as well as the effects of encapsulation on the bubble dynamics for biomedical applications.[13] Bubble oscillations have been investigated inside viscoelastic media with linear viscoelastic models[14–17] which are suitable for small deformation of the medium, and nonlinear viscoelastic models,[18–22] applicable also for large

[a] *Department of Chemical Engineering, Imperial College London, London SW7 2AZ, UK. E-mail: v.garbin@imperial.ac.uk*

[b] *Laboratoire Charles Coulomb (L2C), UMR 5221 CNRS-Université de Montpellier, Montpellier, France*

material deformation. Numerical simulations based on linear constitutive models have shown that in viscoelastic solids the amplitude of the radial oscillations is hindered by elasticity,[16] whereas it is increased in viscoelastic liquids.[14] The elasticity of the medium can also induce a qualitative change in the bubble dynamics compared to a Newtonian fluid, producing, for example, a modulated radial response.[14] Numerical studies based on nonlinear constitutive equations and large-amplitude ultrasound forcing show even more complex bubble dynamics, such as aperiodic oscillations and chaotic behavior.[19–22] It is also found that the threshold for inertial cavitation is greatly reduced as the fluid elasticity is increased,[18,22] with potential implications for biomedical applications.

These theoretical studies have provided important insights into bubble dynamics in viscoelastic media, but experimental data remain sparse, and careful validation of the applicability of constitutive models has not been performed. A recent study has employed oscillatory bubble dynamics in ultrasound to infer the rheological properties of a soft viscoelastic solid (gelatin).[23] Spherical bubbles were created using a pulsed laser inside gels supersaturated with gas. The bubble radius slowly increased over time due to gas transfer into the bubble, and the response as a function of equilibrium bubble radius was measured using a constant excitation frequency of 28 kHz. From a linear analysis of bubble dynamics using the Kelvin–Voigt model, values of shear modulus and shear viscosity were extracted. Because the properties were found to differ depending on the confinement conditions (isolated bubble, bubble near a solid boundary, bubble near a second bubble) the validity of the assumption of linear viscoelasticity should be tested. In ref. 23, the properties were compared with literature values measured at different frequencies[24,25] and the samples used in the experiments were not characterised independently using standard rheological methods.

In this paper we examine the ultrasound-driven oscillatory dynamics of spherical bubbles embedded in soft viscoelastic solids. We make agarose gels with different rheological properties by tuning the agarose concentration, and characterise the samples by rotational rheometry. We inject isolated bubbles inside the gels, and record their radial dynamics under ultrasonic forcing using high-speed video microscopy. We develop a test for linear deformation applicable to bubble oscillations, so that strain amplitudes in the linear regime can be used. We then characterise experimentally the resonant behaviour of bubbles, and analyse the data using linear theory based on the Rayleigh–Plesset equation for bubble dynamics, and the Kelvin–Voigt model for the material deformation. The rheological properties extracted from bubble dynamics are compared with those obtained with the rheometer. The validity of the assumption of linear viscoelasticity is carefully tested.

2 Theory

Consider a spherical bubble in an incompressible, homogeneous, viscoelastic medium. We define a spherical coordinate system

with origin at the centre of the bubble, with r, θ, and ϕ the radial, azimuthal, and polar coordinates respectively. During acoustic driving, the bubble undergoes volumetric oscillations, expanding and compressing at the frequency of the acoustic pressure oscillations. The motion of the bubble generates in the surrounding medium a velocity field $\underline{u} = (u_r, u_\theta, u_\phi)$, with $u_r = \dot{R}(R/r)^2$, and $u_\theta = u_\phi = 0$.[12] The time evolution of the bubble radius, R, is governed by the generalised Rayleigh–Plesset equation:[26]

$$\rho\left(R\ddot{R} + \frac{3}{2}\dot{R}^2\right) = p(R) - p_\infty + \int_R^\infty \left|\nabla \cdot \underline{\underline{\tau}}\right|_r \mathrm{d}r, \qquad (1)$$

valid for any rheology of the surrounding medium. The dots denote differentiation with respect to time, ρ is the density of the medium, p_∞ the pressure far from the bubble, and $\left|\nabla \cdot \underline{\underline{\tau}}\right|_r = \frac{1}{r^2}\frac{\partial}{\partial r}(r^2\tau_{rr}) - \frac{\tau_{\theta\theta} + \tau_{\phi\phi}}{r}$ is the radial component of the divergence of the deviatoric stress tensor, $\underline{\underline{\tau}}$.

The pressure in the medium at the interface, $p(R)$, is related to the balance of normal stresses at the interface of the bubble:

$$p(R) + \frac{2\sigma}{R} - \tau_{rr}(R) = p_{\mathrm{gas}}(R), \qquad (2)$$

where σ is the interfacial tension, τ_{rr} is the radial component of the stress tensor in the medium, and p_{gas} is the gas pressure inside the bubble.

In the linear regime of deformation of a viscoelastic medium, $\underline{\underline{\tau}}$ is traceless, $\tau_{\theta\theta} + \tau_{\phi\phi} = -\tau_{rr}$, and $\left|\nabla \cdot \underline{\underline{\tau}}\right|_r$ becomes

$$\left|\nabla \cdot \underline{\underline{\tau}}\right|_r = \frac{\partial \tau_{rr}}{\partial r} + \frac{3\tau_{rr}}{r}. \qquad (3)$$

With these assumptions, eqn (1), simplifies to:[26]

$$\rho\left(R\ddot{R} + \frac{3}{2}\dot{R}^2\right) = p_{\mathrm{gas}}(R) - p_\infty - \frac{2\sigma}{R} + 3\int_R^\infty \frac{\tau_{rr}}{r}\mathrm{d}r. \qquad (4)$$

We now specify the constitutive model for the viscoelastic medium, which relates the stress tensor, $\underline{\underline{\tau}}$, to the strain tensor, $\underline{\underline{\varepsilon}}$, and the rate of strain tensor, $\underline{\underline{\dot{\varepsilon}}}$. The Kelvin–Voigt model for the linear deformation of an incompressible viscoelastic solid reads:

$$\underline{\underline{\tau}} = G\left(\underline{\underline{\varepsilon}} + \underline{\underline{\varepsilon}}^T\right) + \mu\left(\underline{\underline{\dot{\varepsilon}}} + \underline{\underline{\dot{\varepsilon}}}^T\right), \qquad (5)$$

where G is the shear modulus and μ the shear viscosity. The radial component of the stress tensor, τ_{rr}, is then simply given by

$$\tau_{rr} = 2(G\varepsilon_{rr} + \mu\dot{\varepsilon}_{rr}), \qquad (6)$$

where $\dot{\varepsilon}_{rr} = \partial u_r/\partial r = -2R^2\dot{R}/r^3$, and $\varepsilon_{rr} = -2(R^3 - R_0^3)/3r^3$. Note that the strain and strain rate are not homogeneous, and decay as r^{-3}. Evaluating the integral in eqn (4) yields:

$$\rho\left(R\ddot{R} + \frac{3}{2}\dot{R}^2\right) = p_{\mathrm{gas}}(R) - p_\infty - \frac{2\sigma}{R} - \frac{4\mu\dot{R}}{R} - \frac{4G}{3}\left(\frac{R^3 - R_0^3}{R^3}\right). \qquad (7)$$

The pressure far from the bubble is $p_\infty = p_0 + p_a(t)$, where p_0 is the ambient pressure, and the acoustic pressure

$p_a(t) = \Delta p \sin(\omega t)$ has amplitude Δp and frequency $\omega = 2\pi f$. We assume the gas pressure to follow a polytropic relationship, $p_{gas} = p_{gas,0}\left(\dfrac{R_0}{R}\right)^{3\kappa}$, where R_0 is the bubble radius at equilibrium and κ the polytropic exponent.[27] The gas pressure at equilibrium is $p_{gas,0} = p_0 + 2\sigma/R_0$, where p_0 is the ambient pressure. In Appendix we calculate the value of κ for the bubble size and frequency range used in our experiments.

For sufficiently small forcing amplitude, $\Delta p/p_0 \ll 1$, the radial response, $R(t) = R_0[1 + x(t)]$, can be assumed to follow the same temporal dependence as the forcing, $x(t) = x_0 \sin(\omega t + \varphi)$, where the amplitude of oscillations is small, $x_0 = \Delta R/R_0 \ll 1$, and φ is the phase shift between the forcing and the oscillations. Under these assumptions, linearisation of eqn (7) returns the equation for the amplitude x in the form of a damped harmonic oscillator:[27]

$$\ddot{x} + 2\beta\dot{x} + \omega_0^2 x = \frac{\Delta p}{\rho R_0^2}\sin(\omega t), \tag{8}$$

where ω_0 is the natural frequency,[23] given by:

$$\omega_0^2 = \frac{3\kappa p_0 + \dfrac{2\sigma}{R_0}(3\kappa - 1) + 4G}{\rho R_0^2}, \tag{9}$$

and β is the damping coefficient. If surface tension and elasticity are neglected, the Minnaert frequency is recovered. The only damping mechanism included in this model is viscous dissipation, hence[27] $\beta = \beta_{vis} = \dfrac{2\mu}{\rho R_0^2}$. A comparison of the magnitudes of viscous, thermal, and acoustic contributions to damping shows that this assumption is justified (see Appendix).

The amplitude of bubble oscillations as a function of the applied frequency is given by:[28]

$$x_0(\omega) = \frac{\Delta p/\rho R_0^2}{\sqrt{\left(\omega_0^2 - \omega^2\right)^2 + 4\beta^2\omega^2}}, \tag{10}$$

which describes the resonance behaviour of the system. In the presence of damping, the resonance frequency, for which the amplitude of oscillations is a maximum, is given by:

$$\omega_{res}^2 = \omega_0^2\left(1 - \frac{2\beta^2}{\omega_0^2}\right). \tag{11}$$

3 Materials and methods

3.1 Gel preparation and characterisation

The viscoelastic solids used in this study are agarose gels. The rheological properties of the gels were tuned through the concentration of agarose. Gels were prepared by mixing desired amounts of agarose powder (Sigma-Aldrich, A9539) with ultra pure water (Milli-Q filtration system, Millipore) and glycerol (Sigma-Aldrich, G9012), with a glycerol to water ratio of 3 : 2 v/v. The mixture was left to stir and boil at 95 °C until the solution became clear. The mixture was poured into a container and left to set for 4 hours. The gel samples were characterised using a rotational rheometer (MCR 302, Anton Paar) with a parallel plate configuration. The gap between the plates, which were 25 mm in radius, was set to 7 mm, resulting in a minimum strain of $2.8 \times 10^{-6}\%$ and a minimum torque of 0.5 nN m. The shear modulus, G, was obtained from a stress relaxation test, while the storage and loss moduli, G' and G'' respectively, were measured at a frequency $\omega = 2\pi$ rad s^{-1}. Furthermore, the typical duration of a measurement, of the order of 10^{-4} s, is much smaller than the poroelastic relaxation time, estimated to be 0.5 s[29,30] with the assumption of a mesh size of 500 nm for agarose.[29]

3.2 Injection of isolated bubbles

Isolated bubbles with radii in the range 100–220 μm were injected using a silica capillary with inner diameter of 50 μm and outer diameter of 192 μm (TSP050192, CM Scientific) connected to a compressed nitrogen outlet operating at 0.5 bar. The bubbles were injected in the gel through a hole in the side of the container as the gel was setting. Since the gelation temperature depends on gel concentration, bubble injection temperatures for each concentration were determined by trial and error (24.5 °C, 25.5 °C, and 26.5 °C for 0.5% 1% and 2% respectively). The use of a water–glycerol mixture was found to prevent bubble rise during setting of the gel. It also prevented bubble dissolution, which would lead to the formation of a liquid-filled cavity around the bubble, as observed in ref. 23. The gel samples were $25 \times 35 \times 15$ mm^3, and the bubble was always at least 7 mm from any of the surfaces.

3.3 Experimental setup

Fig. 1 shows a schematic of the experimental setup. A single-element piezoelectric transducer (P-121.05, Physik Instrumente) was glued to a glass slide, which was positioned on the stage of an inverted microscope (IX71, Olympus) equipped with a 4× objective. The agarose gel sample was positioned on the glass slide in the optical window of the microscope stage. The waveform driving the piezoelectric transducer was generated by an arbitrary waveform generator (33220A, Agilent) and amplified by a linear radio-frequency power amplifier (AG1021, T&C Power Conversion Inc.). The waveform consisted of a single burst of 10 cycles at a frequency in the range 10–50 kHz, with amplitude modulated by a sine envelope to prevent windowing effects. The bubble dynamics were captured using a high-speed camera (Photron, FASTCAM SA5) at 300 000 frames per second. Simultaneous triggering of the waveform generator and the high-speed camera was achieved using a pulse-delay generator (9200 Sapphire, Quantum Composer). The pressure generated by the piezoelectric transducer was calibrated using a PVDF hydrophone (RP 33 s, RP Acoustics). The degree of power amplification was adjusted to compensate for the frequency-dependent response of the transducer, so as to maintain a constant pressure for the different frequencies used. A direct measurement of pressure at the location of the bubble could not be performed, because the hydrophone does not provide reliable measurements inside the solid-like gels used for this study. In addition, the repeatability in the position of the bubble is limited,
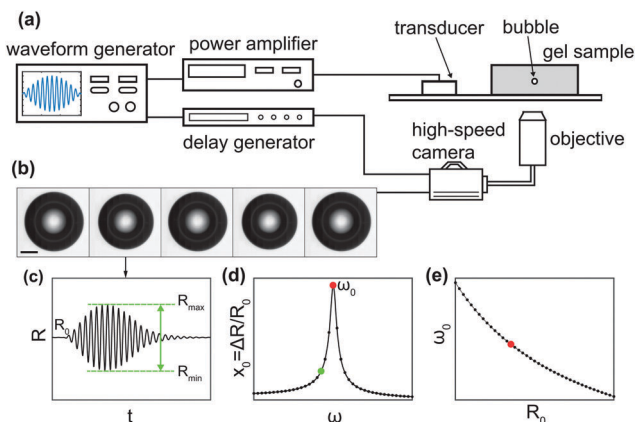
Fig. 1 Schematic of the experimental setup and methods. (a) Acoustical-optical setup. (b) Image sequence of bubble undergoing oscillations at 18 kHz (scale bar 100 μm). (c) Time evolution of bubble radius, $R(t)$, with R_{max} and R_{min} indicated by the horizontal dashed lines. R_0 is the equilibrium radius. (d) Resonance curve: each point corresponds to a measurement of $\Delta R = (R_{max} - R_{min})/2$ for different forcing frequency ω. The maximum amplitude is for $\omega \approx \omega_0$, indicated in red, where ω_0 is the natural frequency of the bubble. (e) Natural frequency ω_0 as a function of equilibrium radius R_0: each point is obtained from the resonance curve of a bubble with different R_0.

and the sound field inside the gel is not homogeneous. The pressure amplitude Δp will be inferred from the analysis of bubble dynamics using eqn (10).

3.4 Data acquisition and processing

We used an acoustic spectroscopy method[31] to experimentally characterise the resonant behaviour of bubbles in an acoustic field, as illustrated in Fig. 1(b–d). Each bubble was repeatedly driven by 10-cycle bursts with increasing frequency in the range f = 10–50 kHz in steps of 1 kHz. An optical recording of the bubble dynamics was taken for each frequency, see Fig. 1(b). The waiting time between subsequent bursts was limited by the download time of the camera sensor to about 10 s. This delay ensured that, if the gel properties were in any way altered by the bubble oscillations, the material had sufficient time to relax back to its equilibrium state before the next recording (see Section 4.1). Each video was analysed frame by frame using built-in edge detection routines in Matlab (MathWorks), to extract the bubble radius as a function of time, $R(t)$, see Fig. 1(c). The amplitude of oscillations was quantified from each video as $\Delta R = (R_{max} - R_{min})/2$, where R_{max} and R_{min} are the maximum and minimum values of the radius. By measuring this quantity for each driving frequency, we reconstruct experimentally the resonance curve, see Fig. 1(d). The uncertainty on the radius is quantified from the standard deviation of a dataset where ultrasound is not applied and the bubble has constant radius. No significant change in the bubble radius due to rectified diffusion[32] was observed over the duration of an experiment, to within the experimental uncertainty. Since we characterised the resonant behaviour of bubbles with a range of sizes, we also analysed the bubble natural frequency, ω_0, as a function of bubble radius, R_0, as shown in Fig. 1(e).

4 Results and discussion

4.1 Gel characterisation with rotational rheometer

The results of amplitude sweeps and frequency sweeps on gel samples with concentrations 0.5% w/v, 1% w/v, and 2% w/v, are presented in Fig. 2. From the amplitude sweeps in Fig. 2(a), measured at a frequency $\omega = 2\pi$ rad s^{-1}, it can be seen that the storage modulus, G' (solid symbols), is larger than the loss modulus, G'' (open symbols), for all three gel concentrations. This observation indicates that the materials behave predominantly like solids. The response of the gels is linear up to a shear strain amplitude $\varepsilon_{xy} \approx 0.1\%$. From the frequency sweeps in Fig. 2(b), measured with ε_{xy} = 0.06%, it can be seen that the storage modulus, G', is constant over the range of frequencies accessible with the rheometer, justifying the use of the Kelvin–Voigt model to describe its deformation. For the purpose of comparison with the values that will be obtained from bubble dynamics, we present a summary of the rheological properties for the three gel concentrations in Table 1. The observed ratio of one order of magnitude between G' and G'' is similar to that reported for other tissue-mimicking phantoms,[33,34] and representative of the behaviour of a range of biological tissues.[35,36] The shear viscosity is estimated as $\mu \approx G''/\omega$. We can estimate the characteristic time for the material to relax after a stress is removed as $\tau \approx \mu/G$. The characteristic times for the three gels are all of the order of $\tau \sim 10^{-2}$ s. The waiting time between repeat experiments on the same bubble, of the order of seconds, is therefore sufficient for the material to relax to its equilibrium state.
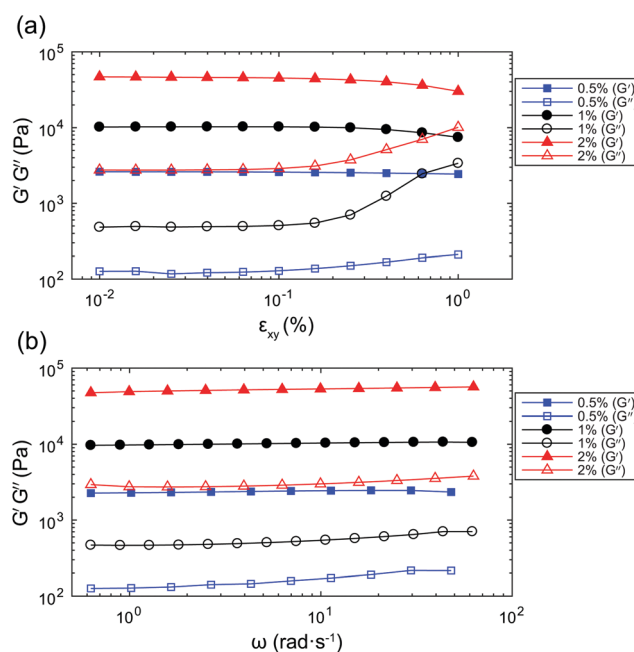
Fig. 2 (a) Amplitude sweep for 0.5%, 1% and 2% gels, measured for shear strain amplitudes ε_{xy} = 0.01–1% at $\omega = 2\pi$ rad s^{-1}. (b) Frequency sweep for 0.5%, 1% and 2% gels, measured for $\omega = (0.1 - 1)2\pi$ rad s^{-1} at a shear strain amplitude ε_{xy} = 0.06%. G' (solid symbols) is the storage modulus and G'' (open symbols) is the loss modulus.

Table 1 Viscoelastic properties of agarose gels with 0.5%, 1% and 2% w/v concentration, measured by stress relaxation test and oscillatory rheometry at f = 1 Hz

Gel concentration (w/v)	0.5%	1%	2%
G (kPa)	2.37 ± 0.05	9.09 ± 0.28	43.53 ± 0.31
G' at 1 Hz (kPa)	2.61 ± 0.14	10.02 ± 0.76	46.67 ± 0.72
G'' at 1 Hz (kPa)	0.126 ± 0.017	0.482 ± 0.041	2.753 ± 0.261
$\mu \approx G''/\omega$ at 1 Hz (Pa s)	20.1 ± 2.7	76.7 ± 6.5	438.2 ± 41.5

Note that the deformation imparted with the rotational rheometer is pure shear with amplitude ε_{xy}, whereas the bubble imparts purely extensional deformation to the material with amplitude $\varepsilon_{rr}(r)$. If the deformation is in the linear regime, shear and extensional rheological tests return the same properties.[37] However, the range of strain amplitudes that corresponds to the linear regime can be different for the two modes of deformation. The maximum strain amplitude for the linear regime of extensional deformation will be determined in the bubble dynamics experiments.

4.2 Gel characterisation from bubble dynamics

4.2.1 Test for linear regime.
The bubble dynamics are expected to be linear for sufficiently small forcing amplitude, $\Delta p/p_0 \ll 1$, and for a deformation of the viscoelastic medium in the linear regime. A non-linear material response will result in non-linear bubble oscillations, even for forcing amplitudes that would result in linear bubble behaviour in Newtonian fluids, as has been reported for bubbles with a viscolelastic coating.[38] We can therefore determine the maximum strain amplitude for the linear regime of extensional deformation by testing for linearity of the bubble dynamics. The test for linear bubble response is simply based on the analogy with a harmonic oscillator: for a linear oscillator, if the driving amplitude changes by a certain ratio, the amplitude of the response changes by the same ratio. For each gel, we subjected a bubble to 8 ultrasound bursts of 10 cycles, with increasing amplitude Δp_i (i = 1–8) and measured the amplitude of radial oscillations ΔR_i. The bubbles were excited near their Minnaert frequency.

In Fig. 3 we plot the ratio of amplitudes of oscillations $\Delta R_i/\Delta R_1$ as a function of the ratio of forcing amplitudes $\Delta p_i/\Delta p_1$. The ranges of extensional strain amplitudes applied, evaluated at the bubble interface, $\varepsilon_R = \varepsilon_{rr}(R)$, were $\varepsilon_R \approx$ 0.006–0.027, $\varepsilon_R \approx$ 0.009–0.035, and $\varepsilon_R \approx$ 0.001–0.003 for the 0.5%, 1% and 2% gels, respectively. For a perfectly linear material response, we expect a linear correlation with coefficient 1. We fit the data to a quadratic relationship,

$$\frac{\Delta R_i}{\Delta R_1} = a\left(\frac{\Delta p_i}{\Delta p_1}\right)^2 + b\left(\frac{\Delta p_i}{\Delta p_1}\right),$$

to quantify the deviation from linearity. The coefficient b is approximately 1 for the 1% gel (b = 0.997), with negligible deviations from linearity (a = 0.083). The 0.5% and 2% gels exhibit slightly non-linear behaviour (b = 0.958 and a = 0.161; b = 0.733 and a = 0.217, respectively) even for the very small strain amplitudes used. Because it is not possible to further reduce the strain amplitude (which is related to ΔR) within the optical resolution of the experiment, we will work in this regime, keeping in mind that small deviations from linear behaviour can be expected.
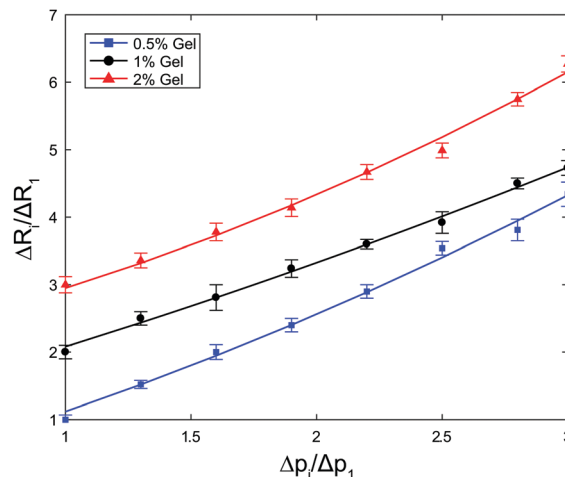
Fig. 3 Test for linearity: $\Delta R_i/\Delta R_1$ is the ratio of amplitudes of oscillations, $\Delta p_i/\Delta p_1$ is the ratio of forcing amplitudes. The 1% and 2% gels are offset by 1 and 2, respectively.

4.2.2 Resonance curves of bubbles in viscoelastic material.
We characterised the resonant behaviour of isolated bubbles in the three gels, using sufficiently small strain amplitudes (determined in Section 4.2.1) to ensure the bubble dynamics were in the linear regime. In Fig. 4 we compare resonance curves obtained in each gel for bubbles of similar equilibrium radius (R_0 = 180, 178, and 171 μm in 0.5%, 1% and 2% gel, respectively) so that qualitative changes in behaviour due to viscoelastic properties of the material can be highlighted. For the purpose of this comparison, the three resonance curves should also have been measured for the same acoustic pressure amplitude Δp. However, to obtain oscillations of measurable amplitude in the 2% gel when driving the bubble off resonance, a slightly larger pressure had to be used than for the other two gels. The comparison of the three resonance curves shows a clear increase in resonance frequency with increasing concentration of the gel, owing to the increase in elasticity. In addition, the peak broadens with increasing gel concentration, due to the increase in viscous dissipation. The amplitude of the resonance curve is also expected to decrease due to the increase in viscous dissipation. This trend is indeed observed, even though the forcing amplitude for the
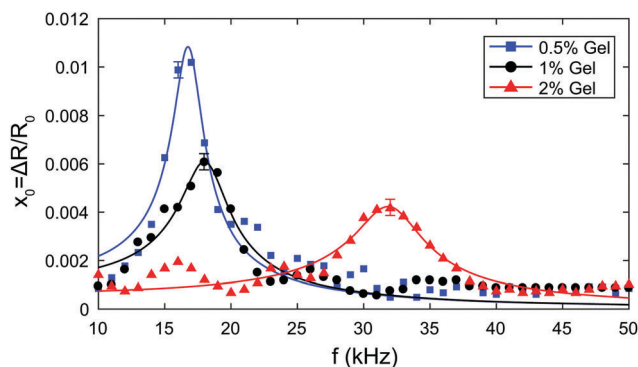
Fig. 4 Resonance curves in 0.5%, 1% and 2% gels respectively. The solid line is a fit of eqn (10) to the experimental data.

Table 2 Viscoelastic properties of agarose gels extracted from ultrasound-driven bubble dynamics at f = 10–50 kHz

Gel concentration (w/v)	0.5%	1%	2%
Pressure amplitude Δp (Pa)	642 ± 47	624 ± 73	956 ± 71
Shear modulus G (kPa)	7 ± 3	21 ± 6	256 ± 29
Shear viscosity μ (Pa s)	0.144 ± 0.016	0.231 ± 0.029	0.280 ± 0.030

2% gel was larger, and therefore no quantitative comparison can be performed. For the 2% gel we observe a subharmonic peak at half the resonance frequency, a manifestation of deviation from linear response.

We can fit eqn (10) to each resonance curve, and extract the values of acoustic pressure amplitude Δp, shear modulus G, and shear viscosity μ from the bubble dynamics data. The results of the fits are summarised in Table 2. The pressure amplitudes are Δp = (642 ± 47) Pa, (624 ± 73) Pa, and (956 ± 71) Pa for the 0.5%, 1% and 2% gels respectively. The values of shear modulus and shear viscosity obtained from the fit of bubble dynamics data are G = (7 ± 3) kPa, (21 ± 6) kPa, and (256 ± 10) kPa, and μ = (144 ± 16) mPa s, (231 ± 29) mPa s, and (280 ± 30) mPa s for the 0.5%, 1% and 2% gels respectively.

To confirm repeatability, resonance curves were measured for over 40 bubbles of different sizes in different gel samples. The results can be summarised by plotting, for each bubble, the value of resonance frequency measured from the resonance curve as a function of the equilibrium bubble radius (Fig. 5). The error bars in Fig. 5 correspond to the width of the resonance curve at 90% of its maximum amplitude. By fitting eqn (9) to the data sets for each gel concentration, we obtain global values for the shear modulus G. The values are consistent with those reported above for a single resonance curve: G = (8 ± 7) kPa, (39 ± 10) kPa, and (239 ± 45) kPa for 0.5%, 1% and 2% gels respectively. Note that the shift in resonance frequency due to viscous damping, given in eqn (11), is negligible and therefore eqn (9) for the natural frequency was used.

4.3 Comparison of viscoelastic properties measured with rheometer and from bubble dynamics

The values of viscoelastic properties obtained from the fit of bubble dynamics data, which are measured at 10–50 kHz, differ significantly

Fig. 5 Summary of experimental data for all bubbles: resonance frequency as a function of bubble radius for each gel concentration. The solid line is a fit to eqn (9).

from those obtained with the rheometer at 1 Hz. The values of G are 2–5 times larger, while the values of μ are two orders of magnitude smaller. We checked that fitting the bubble dynamics data to eqn (9) using fixed values of G and μ from the rheometer measurements, and with Δp as the only fitting parameter, is not possible for any value of Δp. In experiments on bubble dynamics near viscoelastic boundaries, Tinguely et al. measured the shear modulus of agarose hydrogels from the propagation velocity of surface elastic waves.[39] The resulting values of G corresponded to a frequency of deformation of 17–20 kHz, and were found to be 5–30 times larger than the values obtained from a creep test (0 Hz).

We have confirmed experimentally that the bubble dynamics are, to a good approximation, in the linear regime, hence the material response is linear. The difference in the properties measured at high and low frequency therefore suggests that a Kelvin–Voigt model with a single characteristic time is not sufficient to accurately describe the material behaviour over 5 decades in frequency. More complex constitutive linear models will be required to extend the applicability of the modified Rayleigh–Plesset equation over a broad range of frequencies, which can be accessed by probing the dynamics of bubbles of different sizes.

We also found that the bubble dynamics in a viscoelastic medium remain linear only up to a very small amplitude of deformation. The maximum strain rates for the linear regime of extensional deformation [see Fig. 3] correspond to a maximum radial excursion, $\Delta R/R_0$, of the order of 1%. Thus, care should be used in employing linear viscoelastic models for large-amplitude bubble oscillations.

5 Conclusions

We have characterised the resonant behaviour of ultrasound-driven microbubbles in a viscoelastic solid, agarose gel, commonly used as a tissue-mimicking phantom for biomedical applications. Gels with different properties were first characterised by standard rheological tests to obtain the zero-frequency shear modulus G, and the storage and loss moduli, G' and G'', at a frequency f = 1 Hz. Isolated bubbles embedded in the gels were excited by ultrasound at f = 10–50 kHz, and their response was recorded optically using high-speed video microscopy. We used small forcing amplitudes to ensure that the bubble dynamics, and therefore the deformation of the material, remained in the linear regime. Resonance curves obtained experimentally were analysed in the framework of the Rayleigh–Plesset equation, combined with the Kelvin–Voigt model to account for the rheology of the medium, to extract values of shear modulus, G, and shear viscosity, μ. The resonance frequency of the bubbles was found to increase
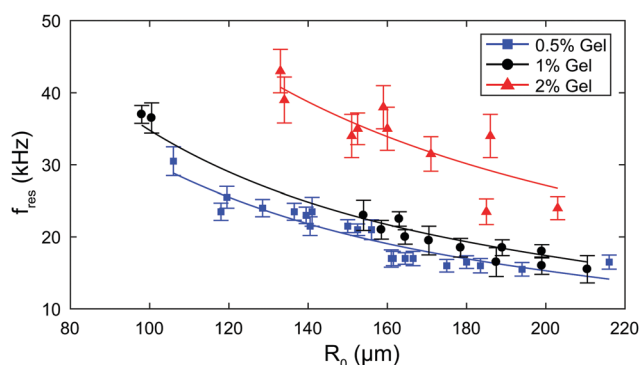
with increasing shear modulus of the medium. This finding implies that imaging and therapeutic ultrasound protocols need to be optimised depending upon the tissue in which the bubbles are embedded. The values of G and μ obtained from bubble dynamics differ significantly from those measured with the rheometer. This finding clearly shows that, even in the linear regime, material properties measured at high frequency can be completely different to those measured with conventional rheometers. Hence, rheological characterisation of biomaterials for medical ultrasound applications requires particular attention to the strain rate applied. Oscillatory deformation imparted by ultrasound-driven bubble dynamics can be used to measure rheological properties in the frequency range that is used in imaging and therapeutic ultrasound. This method can be extended to non-linear bubble oscillations, so long as the bubble remains spherical, and to materials with highly non-linear response. The experimental validation of non-linear constitutive models combined with the governing equation of bubble dynamics will be the subject of future studies.

Appendix

Using the equations given in ref. 27, valid for small amplitudes of the acoustic forcing ($\Delta p \ll p_0$), we have calculated the values of the polytropic exponent and of the acoustic and thermal damping coefficients for a bubble of radius $R_0 = 160$ μm, typical of our experiments. The ambient pressure was taken to be $p_0 = 1 \times 10^5$ Pa, and the ratio of specific heats for the gas was approximated with that of an ideal diatomic gas, $\gamma = 1.4$. The interfacial tension was taken to be[40] $\sigma = 67.6 \times 10^{-3}$ N m^{-1}. The values of the other physical properties used for the calculation are summarised in Table 3. The small amount of agarose polymer used (0.5–2% w/v) can be assumed to have negligible effect on density, speed of sound, and the thermal transport properties of the medium. These properties were calculated for the 2 : 3 v/v water : glycerol mixture, without agarose, using data from ref. 40–42. Comparison of the values of thermal conductivity and diffusivity of water and 3% agar gels[43] confirms that the difference is negligible. On the other hand, since the agarose forms a gel, it has a dramatic effect on the viscosity of the medium. We therefore used the value of shear viscosity of the agarose gel, rather than that of the 2 : 3 v/v water : glycerol mixture.

Fig. 6a shows the dependence of the polytropic exponent on frequency. The range of frequencies used in our study is highlighted by the shaded area. Since κ varies slightly over this range, in the model we use its mean value, $\kappa \approx 1.32$.

Table 3 Parameters used for calculation of polytropic exponent, κ, and damping coefficients, β_{vis}, β_{th}, and β_{ac}

Density of medium: ρ	1.168×10^3	kg m^{-3}
Shear viscosity of medium: μ	0.144	Pa s
Speed of sound in medium: c	1.8×10^3	m s^{-1}
Thermal diffusivity in medium: D	1.031×10^{-7}	m^2 s^{-1}
Thermal conductivity of medium: K	0.364	W m^{-1} K^{-1}
Density of air: ρ_g	1.163	kg m^{-3}
Speed of sound in air: c_g	347.36	m s^{-1}
Thermal diffusivity in air: D_g	2.257×10^{-5}	m^2 s^{-1}
Thermal conductivity of air: K_g	0.0263	W m^{-1} K^{-1}
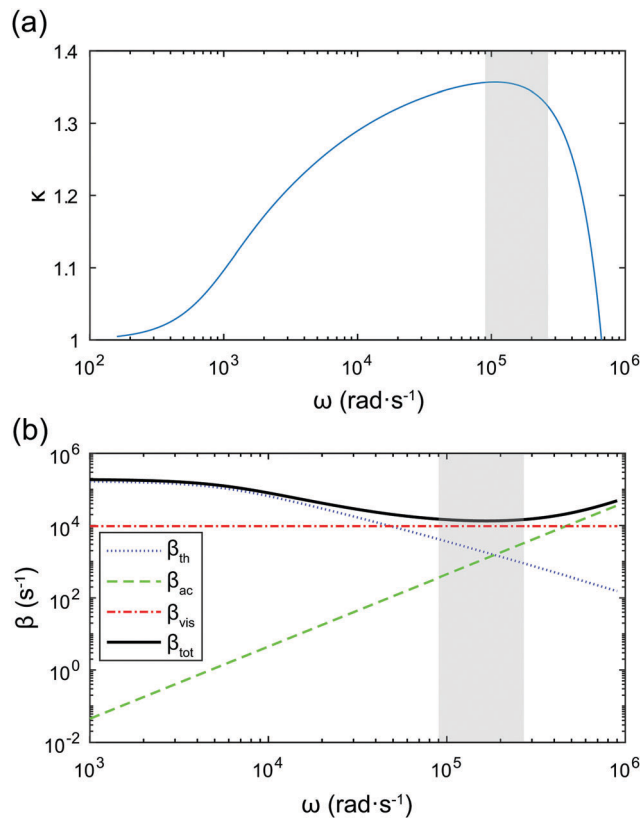
Fig. 6 (a) Dependence of the polytropic exponent on the applied frequency. (b) Comparison of thermal, acoustic, and viscous damping coefficients as a function of frequency. The shaded areas mark the frequency range used in our experiments. The bubble radius is $R_0 = 160$ μm and $p_0 = 1 \times 10^5$ Pa, $\gamma = 1.4$, $\sigma = 67.6 \times 10^{-3}$ N m^{-1}. Other physical properties used for the calculation are given in Table 3.

Radiation of sound by the bubble, and therefore acoustic damping, as well as thermal damping, have been neglected in the model. This assumption can be justified by comparing the viscous damping coefficient, β_{vis}, with the acoustic and thermal damping coefficients, β_{th} and β_{ac} respectively:

$$\beta_{th} = \frac{2\mu_{th}}{\rho R_0^2}, \quad (12)$$

$$\beta_{ac} = \frac{\frac{\omega}{2}\left(\frac{\omega R_0}{c}\right)}{1 + \left(\frac{\omega R_0}{c}\right)^2}, \quad (13)$$

where μ_{th} is a "thermal" viscosity, effectively accounting for thermal dissipation,[27] and c is the speed of sound. Fig. 6b shows the frequency dependence of the three damping coefficients for the same parameters as in Fig. 6a. The shaded area highlights the frequency range used in our experiments. The average values over this frequency range are as follows: $\beta_{vis} \approx 9.6 \times 10^3$ s^{-1}, $\beta_{th} \approx 1.7 \times 10^3$ s^{-1}, $\beta_{ac} \approx 1.7 \times 10^3$ s^{-1}. The viscous damping coefficient is an order of magnitude larger than both the acoustic and thermal damping coefficients, hence the total damping coefficient $\beta_{tot} = \beta_{vis} + \beta_{th} + \beta_{ac}$ is almost entirely accounted for

by viscous damping. These values are obtained using the lowest value of shear viscosity, that is, $\mu \approx 140$ mPa s for the 0.5% gel. Using the values of shear viscosity for the other gels, or the values measured with the rheometer at 1 Hz (see Table 1), shows an even more pronounced dominance of viscous damping.

Acknowledgements

References

1 J. R. B. B. Goldberg and F. Forsberg, *Ultrasound Contrast Agents: Basic Principles and Clinical Applications*, Dunitz, London, 2nd edn, 2001.

2 J. J. Choi, K. Selert, F. Vlachos, A. Wong and E. E. Konofagou, *Proc. Natl. Acad. Sci. U. S. A.*, 2011, **108**, 16539–16544.

3 N. Y. Rapoport, A. M. Kennedy, J. E. Shea, C. L. Scaife and K.-H. Nam, *J. Controlled Release*, 2009, **138**, 268–276.

4 T. O. Matsunaga, P. S. Sheeran, S. Luois, J. E. Streeter, L. B. Mullin, B. Banerjee and P. A. Dayton, *Theranostics*, 2012, **2**, 1185–1198.

5 C. Coussios, C. Farny, G. Ter Haar and R. Roy, *Int. J. Hyperthermia*, 2007, **23**, 105–120.

6 C. C. Coussios and R. A. Roy, *Annu. Rev. Fluid Mech.*, 2008, **40**, 395–420.

7 S. Yoshizawa, T. Ikeda, A. Ito, R. Ota, S. Takagi and Y. Matsumoto, *Med. Biol. Eng. Comput.*, 2009, **47**, 851–860.

8 T. Hall, M. Bilgen, M. Insana and T. Krouskop, *IEEE Trans. Ultrason. Eng.*, 1997, **44**, 1355–1365.

9 S. R. Aglyamov, A. B. Karpiouk, Y. a. Ilinskii, E. a. Zabolotskaya and S. Y. Emelianov, *J. Acoust. Soc. Am.*, 2007, **122**, 1927.

10 A. Karpiouk, S. Aglyamov, Y. Ilinskii, E. Zabolotskaya and S. Emelianov, *IEEE Trans. Ultrason. Eng.*, 2009, **56**, 2380–2387.

11 E. Shirota and K. Ando, *J. Phys.: Conf. Ser.*, 2015, **656**, 012001.

12 M. S. Plesset and A. Prosperetti, *Annu. Rev. Fluid Mech.*, 1977, **9**, 145–185.

13 D. B. Khismatullin and A. Nadim, *Phys. Fluids*, 2002, **14**, 3534.

14 J. S. Allen and R. A. Roy, *J. Acoust. Soc. Am.*, 2000, **107**, 3167.

15 C. Hua and E. Johnsen, *Phys. Fluids*, 2013, **25**, 083101.

16 X. Yang and C. C. Church, *J. Acoust. Soc. Am.*, 2005, **118**, 3595–3606.

17 H. Fogler and J. Goddard, *Phys. Fluids*, 1970, **13**, 1135.

18 J. S. Allen and R. A. Roy, *J. Acoust. Soc. Am.*, 2000, **108**, 1640–1650.

19 J. Naude and F. Mendez, *J. Non-Newtonian Fluid Mech.*, 2008, **155**, 30–38.

20 H. A. Kafiabad and K. Sadeghy, *J. Non-Newtonian Fluid Mech.*, 2010, **165**, 800–811.

21 F. Cunha and D. Albernaz, *J. Non-Newtonian Fluid Mech.*, 2013, **191**, 35–44.

22 J. Jimenez-Fernandez and A. Crespo, *Ultrasonics*, 2005, **43**, 643–651.

23 F. Hamaguchi and K. Ando, *Phys. Fluids*, 2015, **27**, 113103.

24 A. D. Maxwell, C. A. Cain, T. L. Hall, J. B. Fowlkes and Z. Xu, *Ultrasound in medicine & biology*, 2013, **39**, 449–465.

25 S. Yoon, S. R. Aglyamov, A. B. Karpiouk, S. Kim and S. Y. Emelianov, *J. Acoust. Soc. Am.*, 2011, **130**, 2241–2248.

26 A. Prosperetti, *Phys. Fluids*, 1982, **25**, 409–410.

27 A. Prosperetti, *J. Acoust. Soc. Am.*, 1977, **61**, 17.

28 L. Landau and E. M. Lifshitz, *Mechanics*, Butterworth-Heinemann, 1976.

29 J. Narayanan, J.-Y. Xiong and X.-Y. Liu, *J. Phys.: Conf. Ser.*, 2006, **28**, 83–86.

30 W.-C. Lin, K. R. Shull, C.-Y. Hui and Y.-Y. Lin, *J. Chem. Phys.*, 2007, **127**, 094906.

31 S. M. van der Meer, B. Dollet, M. M. Voormolen, C. T. Chin, A. Bouakaz, N. de Jong, M. Versluis and D. Lohse, *J. Acoust. Soc. Am.*, 2007, **121**, 648–656.

32 D. Hsieh, *J. Acoust. Soc. Am.*, 1961, **33**, 206.

33 K. Manickam, R. R. Machireddy and S. Seshadri, *J. Mech. Behav. Biomed. Mater.*, 2014, **35**, 132–143.

34 C. U. Devi, R. M. Vasu and A. K. Sood, *J. Biomed. Opt.*, 2005, **10**, 44020.

35 T. A. Krouskop, T. M. Wheeler, F. Kallel, B. S. Garra and T. Hall, *Ultrasonic imaging*, 1998, **20**, 260–274.

36 M. Zhang, B. Castaneda, Z. Wu, P. Nigwekar, J. V. Joseph, D. J. Rubens and K. J. Parker, *Ultrasound in Medicine and Biology*, 2007, **33**, 1617–1631.

37 C. Macosko, *Rheology: principles, measurements, and applications*.

38 M. Overvelde, V. Garbin, J. Sijl, B. Dollet, N. de Jong, D. Lohse and M. Versluis, *Ultrasound in medicine & biology*, 2010, **36**, 2080–2092.

39 M. Tinguely, M. G. Hennessy, A. Pommella, O. K. Matar and V. Garbin, *Soft Matter*, 2016, **12**, 4247–4256.

40 G. P. Association *et al.*, *Physical properties of glycerine and its solutions*, Glycerine Producers' Association, 1963.

41 J. H. Perry, *J. Chem. Educ.*, 1950, **27**, 533.

42 N.-S. Cheng, *Ind. Eng. Chem. Res.*, 2008, **47**, 3285–3288.

43 R. G. Holt and R. A. Roy, *Ultrasound in Medicine & Biology*, 2001, **27**, 1399–1412.